Efficientnetb0-Optimized Detection: Revolutionary Kidney Cachexia Nutritional Evaluation in Healthcare Innovation

R. Sumathi[1], K. Gunasubha[2], B. Harshini[3], Z. Badhurunnisha[4]

[1,2,3,4]Panimalar Engineering College

Abstract

The identification of kidney illnesses is being revolutionized by deep learning approaches such as Convolutional Neural Networks (CNNs). CNNs are useful tools for analyzing medical imaging data, including ultrasounds and CT scans, and spotting structural anomalies in the kidneys. Conversely, CNNs may create representations of kidney-related features and model intricate data distributions, which aids in the detection of subtle illness patterns. Together, these techniques improve the precision of disease progression forecasts and individualized treatment regimens while facilitating the early detection of diseases such as tumors, stones, and chronic renal disease. Significant progress has been achieved in the early identification, diagnosis, and monitoring of kidney illnesses with the incorporation of deep learning techniques such as Convolutional Neural Networks (CNNs). CNNs are essential for the study of several imaging modalities, including MRIs, CT scans, and ultrasounds, because of their capacity to process high- dimensional image data. These models are very good at differentiating between healthy and diseased tissues, identifying and segmenting kidney structures, and spotting anomalies like tumors, cysts, and stones. CNNs can automate image interpretation by identifying complex patterns in medical images, which could lower human error and improve diagnostic precision. Moreover, by integrating both structural (image-based) and functional (clinical and laboratory- based) data, the combination of CNNs in hybrid models can allow for a more thorough knowledge of kidney health. Because it can both anticipate the possibility of a disease and provide customized therapies based on individual risk factors, this synergy enables a more individualized approach to patient care. This development creates new opportunities for precision medicine, which improves patient outcomes and quality of life by tailoring treatment regimens to the particulars of each patient's renal disease. Future kidney disease detection and treatment will be more precise, quick, and individualized as these methods develop further.

Keywords: Convolutional Neural Networks; Deep Learning; Automated Diagnosis; Hybrid Models

INTRODUCTION

A rising worldwide health concern, kidney diseases—including chronic kidney disease (CKD), kidney stones, and tumors—are frequently discovered later in life, when there are few available treatments. Improving patient outcomes and lessening the strain on healthcare systems need early detection and precise monitoring of these disorders. Laboratory testing and physical examinations are examples of traditional diagnostic techniques that are frequently slow and may not be very sensitive. The promise to transform kidney disease diagnosis has surfaced with the introduction of deep learning, specifically

Convolutional Neural Networks (CNNs). While CNNs offer strong tools for learning intricate data representations and identifying minute patterns in patient data, CNNs are excellent at interpreting medical imagery. When combined, these cutting-edge approaches provide more precise, effective, and individualized ways to identify and track the development of kidney disorders, opening the door for more preventive and focused medical therapies. One of the most deadly is kidney cancer, which is regrettably hard to identify in its early stages using standard clinical methods[1]. Research on renal cancer is currently lacking [2], despite the fact that it is one of the top ten cancers that kill people. In the medical community, a variety of cancer kinds have predominated, delaying the use of contemporary detection and treatment techniques. For decades, patients with kidney cancer have had limited treatment options, and their life expectancy is typically estimated to be less than a year. Therefore, automatic diagnostic tools will assist a physician in rapidly and readily determining the patient's condition and ensuring their survival [3]. Classification techniques are frequently employed in a variety of automated medical diagnostic systems Early kidney disease detection is a challenging task [4]. Chronic renal disease (CKD) affects kidney structure and function, and the instrument can lower the testing pressure [5]. Complications from a longer illness may include nerve damage, anemia, high PB, weak bones, problems with the heart or blood vessels, etc. [6]. Depending on the glomerular filtration rate (GFR) stage, the illness manifests at multiple stages [7]. Early detection and treatment of individuals at risk can prevent the development of chronic kidney disease (CKD), which has risen quickly and is associated with an extremely high risk of cardiovascular and end- stage renal disease. In the preceding phase, the disease can now be efficiently evaluated using machine learning methods [8]. These days, the most used method for detecting kidney disease is machine-predicted analysis. Since it is regarded as one of the health risks of developing and rising nations in their early stages, there are a few side effects of CKD that might not be noticeable until crucial kidney function is compromised. By controlling the underlying cause of the disease in its early stages, CKD therapy aims to reduce the progression of renal risk [9]–[11].Epidemiology is linked to the development of CKD along with numerous other clinical features. Nephrophrologists typically utilize blood and urine tests to check for the use of CKD [12]. Age, obesity, diabetes, and heredity can all have an impact on chronic kidney disease (CKD).Blood tests measure the kidneys' ability to filter blood and remove creati-nine, a waste product of normal muscle breakdown [13]. In contrast, the urine test will show that protein is still present in the urine. Specifically, protein (albumin) is a blood component that the kidney filter typically does not allow to enter the urine [14]. When albumin is detected in the urine, it shows damage to the kidney filters and may be a sign of chronic renal disease. The development of a wireless embedded health monitoring platform that serves as the IoMT portal is described in this article. In order to address the deficiency of health analytics in the current monitoring system, this research proposes several models of early prediction kidney disease analytics that may be integrated into a suggested architectural monitoring system [15]. Generally speaking, different physiological indicators could be used to monitor or evaluate a patient's health. Therefore, relying on the disease's physiological parameters, which are insufficient for identifying or forecasting its emergence, is necessary for challenging chronic conditions like diabetes and renal disease [16].
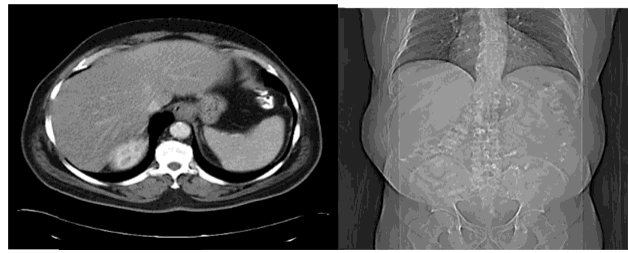
FIGURE 1: (a) Abdominal CT scan of revealed metastatic kidney disease (b) Coronal computed tomography image of Polycystic kidneys [17].

In order to detect and diagnose chronic kidney disease, the Adaptive Hybridized Deep Convolutional Neural Network (AHDCNN) has been proposed in this study. The CNN features that were fed into the support vector machine throughout its development and kidney mitosis observation were extracted using the suggested model. By eliminating features from CT scans, a pre-trained CNN was extensively trained to identify kidney cancer. Figure 1.(a & b) displays the corresponding dataset pictures for the automatic CNN-based magnetic resonant image segmentation system that has been explained. The CNN model's local and global contextual aspects have also been studied. By employing a fully connected layer in the CNN's last layer, the system was able to detect kidney cancer more quickly. Kidney cancer has been segmented using a fully convolutional network and conditional random fields. Initially, the FCN model was trained using picture patches, and conditional random field training was carried out. At last, the image slices have been immediately calibrated by the system. A sophisticated CNN model training approach is combined with adjacent image patches in a single pass. Following CNN's 3D picture segmentation, the fully-connected 3D random field technique has been used to remove false positives[18]-[20].

1. To suggest the Adaptive Hybridized Deep Convolutional Neural Network (AHDCNN) for the diagnosis and prognosis of Chronic Kidney Disease is one of the paper's primary conclusions.
2. To investigate the precision and usefulness of using blood or urine tests to predict chronic kidney disease. Utilize the most significant and representative factors when using machine learning techniques to predict CKD early.
3. The Internet of Medical Things platform was used to conduct the experiment, and the sample datasets were obtained from https://nihcc.app.box.com/v/DeepLesion

The following is how the rest of the paper was represented: The background and current techniques for predicting chronic renal disease were covered in Sections 1 and 2. Section 3 presents a proposal for the early identification and detection of chronic kidney disease using an adaptive hybridized deep convolutional neural network. The experimental results are shown in section 4. Section 5 brings the proposed article to a close.

RELATED WORK

The Neighbourhood Component Analysis (NCA), which uses miRNA genome data to classify kidney cancer subtypes, was proposed by Muhamed Ali et al. [21]. Long Short Term Memory (LSTM), a sort of recurrent neural network, and miRNAs are used to derive discriminative characteristics from the categorization of a particular miRNA sample in kidney cancer subtypes. The NCA process picked dataset 35 of the most biased miRNAs. With an average accuracy of almost 95% and

Matthews' correlation coefficient values of roughly 0.92 under 10 random clustered 5 times, this subset of miRNAs enables LSTM to classify kidney cancer miRNAs into 5 sub-types. These results are extremely near to the average output of all miRNAs for rating purposes. In order to detect and categorize new kidney histologic abnormalities, Sheehan et al. [22] developed the Deep Neural Network (DNN). They show that DNN-based machine learning performs well across a range of histologic image processing tasks. The neural network classified differences between mice of different genotypes by extracting and using quantitative picture information. It was demonstrated that the animal's genotype and non-glomerular segmentation based on quantitative picture attributes performed exceptionally well. These characteristics were not discovered in a systematic pathologic study on the Internet of Medical Things platform (IoMT).The Hybrid Neural Network (HNN) was proposed by Ren et al. [23] as a method for renal disease detection. In order to completely capture the information in Electronic Health Records (EHR), they characterized the prediction issue specifically as a binary classification function. They proposed a hybrid neural network that integrates autoencoding networks with bidirectional long short term memory (BiLSTM). The authors reported creating a data set based on a large portion of the raw EHR data. There are 35,332 reports from hypertensive patients in the collection. According to test results, the suggested neural model achieves 89.7% accuracy on the challenge. The Recurrent Neural Network (RNN) was first developed by Kallenberger and Schmidt [24] in order to predict the onset of acute renal damage. In order for replies to earlier segments of the sequence to be taken into account at a specific point in the series, the RNN will decide the input sequence. RNN predicted the likelihood of Acute Kidney Injury (AKI) in clinical parameter sequences. Approximately 56% of all AKI events would progress clinical diagnosis within 48 hours at the selected point of operation, according to the model, which had a 33% accuracy rate for each of the severity stages of AKI.

This indicates that out of three projected cases, one patient had AKI, whereas the other two had incorrect predictions. Additional testing has revealed that 57% of false-positive estimates have happened in people with chronic renal disease.The Ensembling Multi-stage deep learning approach (EMS-DLA) was presented by Santini et al. [25] for kidney tumor segmentation. The variance between separate models will be subjected to a combining technique in order to incorporate prediction results from earlier stages. On 90 unidentified test cases, the average Dice score for renal and pediatric cancers is 0.96 and 0.74, respectively. Although the results are encouraging, they might be enhanced by accounting for benign cysts, which often reduce tumor segmentation on the Internet of medical things platform (IoMT). This study reports the results, which are drastically reduced. Compared to the smaller batches (8–16) that had been tried earlier, the comparatively large batch size was used, and the batch normalization qualities were better utilized. Among the evaluations, the outcomes of 32 samples improved.This research proposes an adaptive hybridized deep convolutional neural network for the prediction of chronic kidney disease in order to address these problems. Convolution neural networks (CNNs) showed higher performance in a number of computer vision tasks, including object detection, picture recognition, and semantic segmentation.

ADAPTIVE HYBRIDIZED DEEP CONVOLUTIONAL NEURAL NETWORKS(AHDCNN)

This study suggests using the Adaptive Hybridized Deep Convolutional Neural Network (AHDCNN) to predict and diagnose chronic kidney disease.

CNN picture input, the output of each layer has been retrieved to create the image hierarchy features. Through AHDCNN, an accurate segmentation of the integrated system can be achieved in comparison to an FCN by utilizing smoothing and prior information.Additionally, rather than using the model as a post-processing tool, it is integrated into the training phase to modify the CNN. During preparation, it offers the use of unlabeled data in a semi-monitored setting. By training a mapping of MRI signals to hybridized functionality produced from Convolutional Neural Networks, the knowledge of kidney cell activity—in contrast to the MRI signals—has been converted into a CNN understanding of functionality representation. The suggested AHDNN technique architecture is displayed in Figure 2. This study intends to investigate if the tumors may be analyzed by a deep learning model for reliable renal cell rating forecasts from CT (CECT) improvement. The radiography records, which are based on qualified radiology residents of the CECT corticomedullary process, have been used to manually annotate the affected tumors. By adjusting two coefficients in the final two convolutional layers, rectangular ROIs have been selected and utilized as inputs to

the Deep CNN that has already been trained in ImageNet and transfer learning. The ROI extraction of the kidney illness image is displayed in Figure 3.

Preposition 1: A neural feed-forward network, as shown in figure 3.CNN processes the signal directly, without the need for loops or cycles. That can be illustrated like this:

$H(y) = h_M(h_{M-1}(\dots(h_1(Y))))$

$$g_l(y,x) = \sum_{w=-n}^{n}\sum_{r=-u}^{m}\sum_{u=-t}^{s} U_l(w,r,u)\,Y(y-w, x-r, z-u)$$

(1)

Equation (1) illustrates this, with M being the number of hidden layers, Y representing the input signal, and hM denoting the function assigned to layer M. The convolutional layer of a basic CNN model features a function h with several convolutional kernels ($g_1,\dots g_{l-1}, g_l$). Every GL denotes a linear function in the lth kernel represented by the equation that follows.
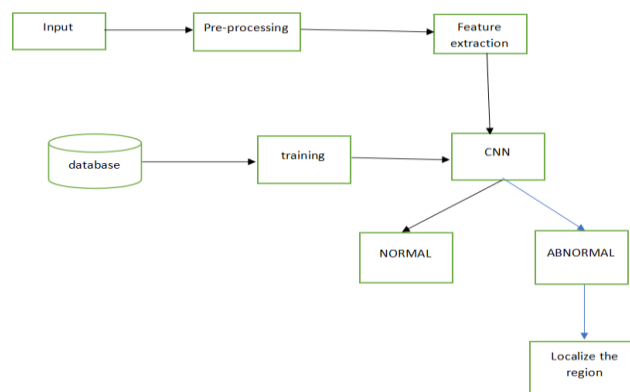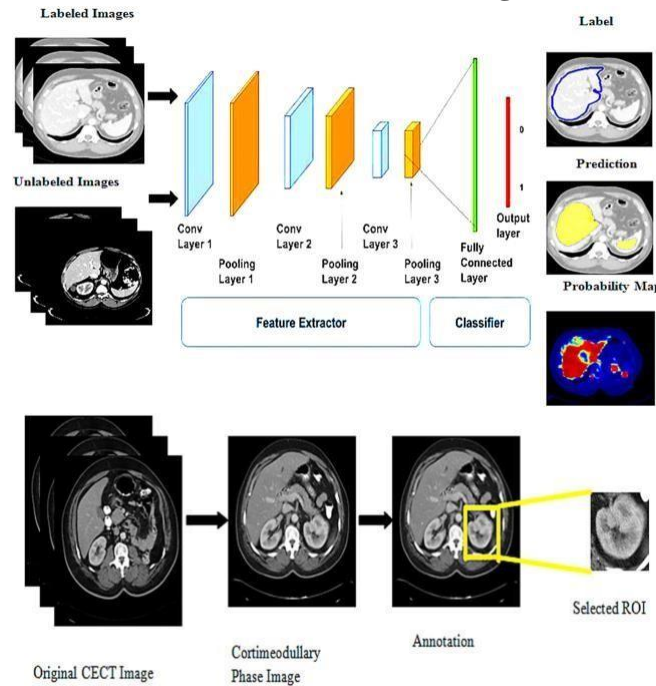

(2)

FIGURE 2: Architecture Diagram

FIGURE 3:Kidney tumour ROI extraction

As demonstrated in equation (2), where (y,x,z) represents the input pixel position Ul stands for the weight of the lth kernel, Y, n for height, m for width, and s for filter depth.The primary role of pooling in CNN is to subsample the neighboring pixels, meaning that they are summed and substituted with the average pooling function. Another form depending on the distance from the center pixel is the weighted average. By pooling, the image becomes invariant to slight changes in the input translation. The Atrous Convolution-marized properties of the findings at a location are indicated by the following equation. This Pooling lowers the dimensionality and invariance of translation and rotary transformations.

Another form depending on the distance from the center pixel is the weighted average. By pooling, the image becomes invariant to slight changes in the input translation.

$$\bar{x}\,[\bar{j}] = \sum_{l=1}^{L} y\,[j + t \cdot l]s[l]$$

(3)

Equation (3) illustrates this, with $y[j]$ representing the 1D input signal, $s[l]$ representing the filter of length l, and t representing the stride rate at which the input signal is sampled. The result of the atrous convolution is $x[j]$. Over the input y, atrous convolution is applied.

The degradation issues that emerge as deep networks converge— that is, the growing complexity of precision loss and degradation—are addressed by deep residual learning. Rather than fitting into a predefined context frame, the residual network makes the layers stack directly to fit into the map. The experimental results accomplish precision with a significant increase in depth and enhance residual network optimization. The problem of disappearance gradients occurs when multiple layers pass through, causing gradient information to be lost. Skip connections provide deep neural networks with transversal

information.

Full pooling eliminates any spatial information, whereas skipping connections provides additional details about the last layer to improve classification accuracy. The activation layer can employ a variety of activation functions, including:

A sigmoid activation function is given by equation (4):

$$\rho(y) = \frac{1}{1 + e^{-y}}$$
(4)

We can combine the layers because the composition is non-linear. Regarding slight changes in the values of x, the range of the y is somewhat sharp, starting at ±2 on the x-axis. There is an abrupt change in the Y values. One benefit of this activation function is that their output stays within the range of (0,1).

Tanh function is stated as follows:

$$f(y) = \tanh(y) = \frac{2}{1 + e^{-4y}} - 1$$

The definition of the scaled sigmoid function is:

$$\tanh(y) = 2\,\mathrm{sigmoid}(2y) - 1 \qquad (6)$$

It is in the range of -1 and 1. Compared to the sigmoid function, the tanh gradient is stronger.

The most commonly employed activation

function denotes a non-linear pixel-wise function, and the g is a Rectified Linear Unit (ReLU). In other words, the output x is provided if x is positive; if not, it is 0.

$$h(y) = \max(0, y) \qquad (7)$$

Since ReLU's combination is non-linear, different layers can be stacked. That activation will also explode because the range is zero to infinity. As a nonlinear layer-sampling function, h reduces the functional size for the pooling layer. The prediction layer is a softmax that forecasts the probability that Yi will and geometric distortions worsen low SNR and artifacts. In order to overcome these obstacles and make it easier to analyze the transplant condition, our segmentation makes use of a number of picture attributes to accurately define the kidney. Typical coronal cross-section MRI samples of (a) low contrast between surrounding and renal abdominal tissues, (b) anatomical variations between patients, (c) image artifacts, and (d) geometric distortion limits are displayed in Figure 4.
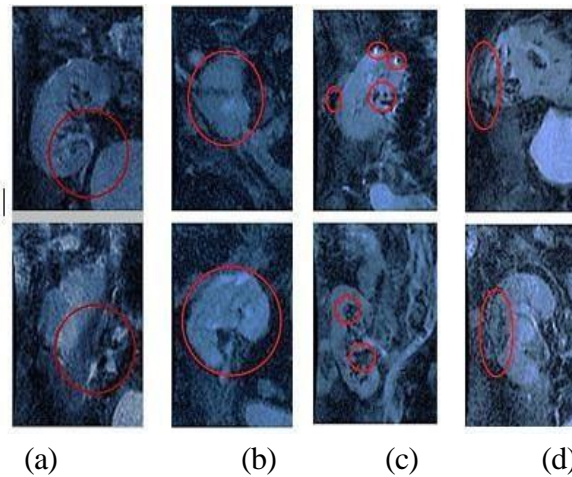
| (a) | (b) | (c) | (d) |

FIGURE 4: . Coronal cross-section MRI sample images (a) low contrast between surrounding and kidney abdominal tissues (b) inter-patient anatomical distinctions (c) image artifacts (d) geomet5. classification of kidney cancer.

Preposition 2 (Mathematical Modeling of Autoencoders): The neural network's unsupervised learning class includes autoencoders. The incoming data teaches them a representation with fewer dimensions. Additionally, the output layer has a straightforward AE structure, while the input layer is followed by a concealed layer. Both the coding and decoding training rounds are finished. The first phase involves using a weight matrix $\Upsilon_{J,I}$ and bias $A_{J,I}$ to encode input J with representations of I.

$$I = \rho \quad \Upsilon_{J,I}J + A_{J,I} \tag{10}$$

as demonstrated by the activation function ρ in equation (10). The following step involves decoding the representation I using the new weight matrix $\Upsilon_{I,\hat{J}}$ and rebuilding $\hat{J}$ using bias $A_{I,\hat{J}}$.

belong to various classes, whereas the 1×1 convolutional kernel $\hat{J} = \rho^r \quad \Upsilon \quad + A_{I,\hat{J}} \tag{11}$

is a fully connected layer. By, iterating from r = 1 to R, CNN estimates the hidden vector sequence f = (f1,... fR) from the input sequence u = (u1,... uR), then computes the output is o=(o1… oR).

$$f_r = F\left(S_{uf}u_r + S_{ff}f_{r-1} + a_f\right) \tag{7)-(8}$$

$$o_r = S_{fo}f_r + a_o$$

As demonstrated in the equations above, where S stands for the bias vectors and the weight matrix. The hidden layer function, or sigmoid function, is denoted by the letter F. Histogram equalization and a non-parametric bias correction are combined in the preprocessing step of the segmentation pipeline to partially eliminate noise and inconsistencies caused by low- frequency non-uniformity intensity inhomogeneity. It is difficult to accurately segment the kidneys because of the following factors: low contrast between the renal and other abdominal images; changes in kidney form due to anatomical differences between patients; and, in particular, higher gradient strengths and lengths. Long acquisition time picture alignment I Ĵ

Equation (11) illustrates this, with ρr serving as the new activation function. One may consider ϒI,Ĵ to be the transpose of ϒJ,I. The purpose of training these autoencoders is to lower the error as

$$\arg\max\ J - \hat{J}^2 \tag{12}$$

Deep convolutional neural networks have accurately predicted the survival period of patients with kidney cancer based solely on the pathology images. A large-scale CNN that has already been trained to detect kidney cancer by removing features from CT scans. They employed 3D CT images for end-to-end testing on CNN multi-view images and 2D CT images to identify kidney nodes. CNN uses the 2D patches that were taken out of the 3D images in order to extract features. The classifier has been fed the characteristics following fusion. The changing nodule size issue is meant to be resolved by this paradigm. By substituting the multi- crop pooling layer for the max-pooling layers in the CNN system, this offers the multi-scale feature.

$$x^k = RReLU \sum_l b^{lk} \times g^l + a^k$$

(13)

Equation (13) illustrates this, with gl representing the lth input map and xl the l-th output map. The convolutional kernel between the kth output map and the lth input map is denoted by blk. The bias of the kth output map is denoted by ak. The formula for RReLU is (10).

$$RReLU = \begin{cases} y \ if \ y \geq 0 \\ \dfrac{y}{c} \ if \ y < 0, \end{cases} \quad c \sim V(a_{k}, a_v)$$

(14)

Equation (14) illustrates this, with V (ak, av) representing the uniform distribution and b representing a random factor drawn from it. The distribution's lower and upper bounds are denoted by ak and av, respectively. The max-pooling that was used is expressed as

$$x^j_{(i,l)} = \max_{0 \leq n,m < w} g^j_{(i-w+n, \ l-w+n)}$$

(15)

As can be seen in equation (15), where w is the pool size, n and m are position offsets, and xj and gji w n l w are the neurons' positions at (i,l) and (i-w+n, l-w+n) in the jth output, respectively. While the normal max pool is utilized for feature subset gathering and map size reduction, the multi-crop pooling technique gathers nodule center features. Therefore, it can be claimed that the pooling process essentially reduces the characteristics by one point. The system is able to accomplish multi-level features in multi-crop pooling through the use of repetitive pooling algorithms. Let's look at the three nodule- centric characteristics that are mixed together and formed from T0, T1, and T2 respectively: f = [f0, f1, f2]. Sizes T0, T1, and T2 are k × k × m, k/2 × k/2 × m, and k/4 × k/4 × m, respectively. The number of features is m.

fj = max − pool$^{(2−j)}$Tj, j = 0, 1, 2 (16)

Equation (16) illustrates this, with max − pool representing the frequency of max pooling on regions Tj. In order for the max pool to produce the feature f0, T1 is the center region cut from T0 once. T0 creates the feature f1 and is the maximum -pooled twice. T2 is a feature f2 that is the center region cropped from T1; it is not max- pooled. These characteristics are concatenated to form a multi-crop. Entropy is minimized for this network's learning and is defined as:

LOSS = − (plogQ1 + (1 − p) log q0) (17)

Equation (17) illustrates this, with p having a suspiciousness value of 0 for low suspicion and 1 for high suspicion. The gradient descent method is used to train the network. One hundred patients with nodules ranging in diameter from 3 to 30 mm make up the dataset. They obtained a 97.14% accuracy rate, a sensitivity of 0.77%, and a specificity of 0.93%. By converting the data into a higher dimensional space, the kernel trick is a mathematical function that turns non-linear, non-separable data into linearly separable data.

L (n, m) = (f (n), f (m)) (18)

When it comes to solely taking into account kidney nodules with renal masses with the hemorrhagic area, as seen in Figure 5(a), the deep model of implementation on the classification of kidney cancer can capture information of interest.
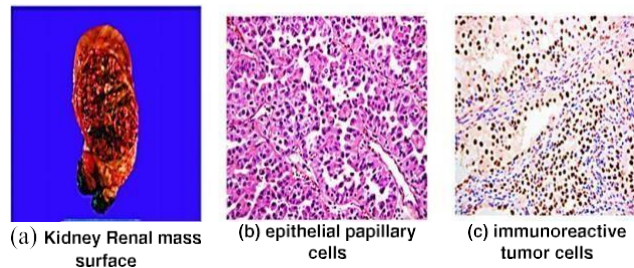
(a) Kidney Renal mass surface　(b) epithelial papillary cells　(c) immunoreactive tumor cells

FIGURE 5:Classification of kidney cancer

To get around this excess information, they computed 26 hand- crafted features and combined them with the detection of CNN- extracted lung nodular epithelial papillary cell features, as seen in Figure 5.(b). The CNN model was used to choose the ground-glass opacity (GGO) candidate regions rather than a pre-trained CNN. The GGO candidate regions were found using the following equation:

$$h(y,x,z) = \sqrt{\left(\frac{\Delta\sigma y}{\Delta y}\right)^2 + \left(\frac{\Delta\sigma x}{\Delta x}\right)^2 + \left(\frac{\Delta\sigma z}{\Delta z}\right)^2}$$

(19)

Equation (19) illustrates how the immunoreactive tumor cells' y, x, and z orientations in figure 5.(c)

$$\Delta\sigma y = |\sigma(y+1,x,z) - \sigma(y,x,z)| + |\sigma(y,x,z) - \sigma(y-1,x,z)| \quad (20)$$

$$\Delta\sigma y = |\sigma(y,x,x+1,z) - \sigma(y,x,z)| + |\sigma(y,x,z) - \sigma(y,x-1,z)| \quad (21)$$

$$\Delta\sigma y = |\sigma(y,x,z+1) - \sigma(y,x,z)| + |\sigma(y,x,z) - \sigma(y,x,z-1)| \quad (22)$$

were calculated using the following formulas:

Labeling techniques have been applied to the morphology, and thresholding techniques have been used to minimize noise for each sphericity of the volume. This operation was completed for the GGO candidates, and the Internet of Medical Things platform (IoMT) was used to analyze the data. According to the simulated outcome, which is displayed as follows, they employed the support vector classification and obtained 93% true positives and 52% false positives.
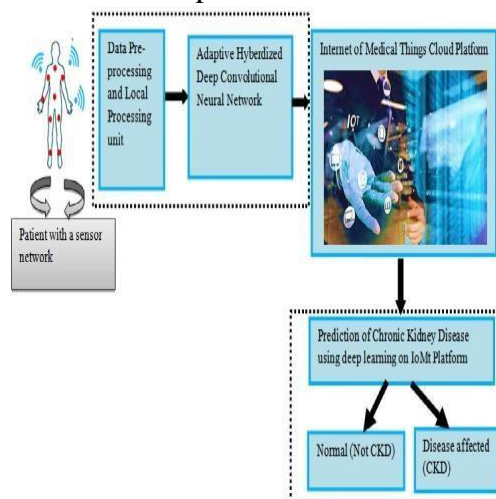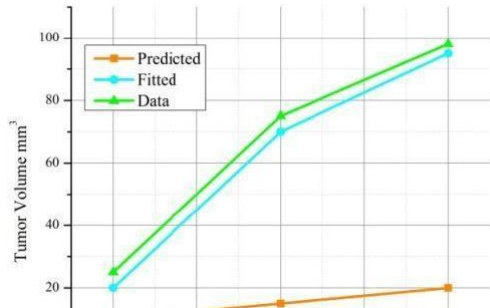

FIGURE 6: Internet of medical things for chronic kidney disease prediction.

EXPERIMENTAL RESULTS:

Prototyping an integrated health care model based on the IoMT model is described in this study. The Internet of Medical Things prediction block diagram for chronic kidney disease is displayed in Figure 6. The forecast findings demonstrate the possibility of including a classification model into the proposed system to identify potential dangers during the early phases of some diseases'therapy. . One example of an Internet of Things solution for healthcare is the use of remote sensors to monitor vital signs and cloud services to provide permanent and real-time information to the appropriate expert. Instead of using a hardwired machine-to-machine (M2M) system with several connected connections that take up valuable space, the Internet of Things uses cloud computing to function as a network for gathering data from sensors. The Internet of Things connects individual devices to the Internet, stores data in the cloud, and shows the collected data on a network-based computer, tablet, or smartphone. Figure 7(a), which displays the input kidney image with varying complexities, provides an example of kidney image segmentation.
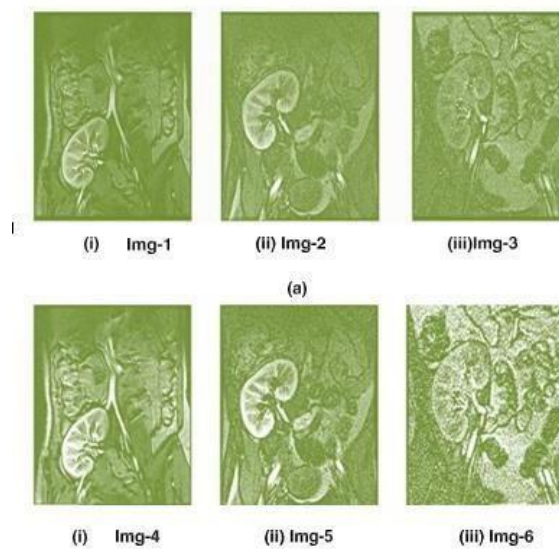

FIGURE 7: (a) Example of kidney image segmentation (a) input kidney images with various complexities (img-1 to img-3) (b) Adjust Intensity values to specified Range(img-4 to img-6).

ACCURACY ANALYSIS FOR NUMERICAL CONSISTENCY:

The integration of processing and deep features. The suggested method incorporates two SVM classifiers: one for robust speed- up features and local binary patterns, and another for raw pictures using deep features obtained from the CNN model and probability scores, as illustrated in Figure 8.(a). The higher scores were used in the final decision.
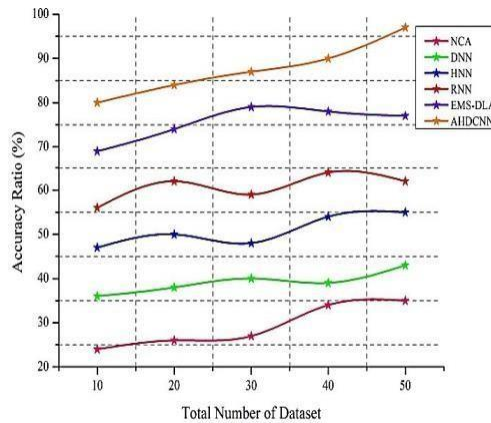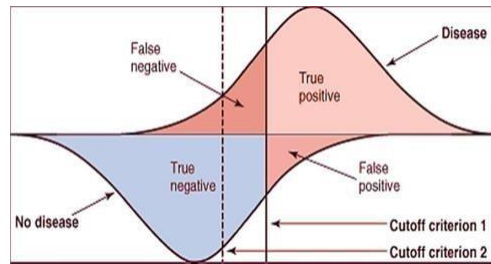
The issues of degradation that arise when the deep network converges—that is, when accuracy reaches saturation and as depth increases—are addressed by deep residual learning. Rather than using the desired frame, the residual network needs the stacked layers to fit directly into the residual maps. With a significant increase in size, the experimental results facilitate the modeling of residual networks and enable the attainment of precision. The growth curve prediction utilizing the suggested AHDCNN is displayed in Figure 8(b), and the accuracy ratio of the suggested AHDCNN approach is displayed in Figure 8(c). As indicated at the bottom of this page, accuracy determines the correct categorization of the number of false-positive FP, false- negative FN, true positive TP, and true negative TN, 23. As a nonlinear layer-sampling function, h reduces the functional size for the pooling layer. The prediction layer is a softmax that predicts the likelihood of Yi belonging to various classes with an accuracy ratio as indicated in the table, while the 1×1 convolutional kernel is a fully connected layer 1

TABLE 1:Accuracy with numerical consistency

Total Number of datasets	NCA	DNN	HNN	RNN	EMS-DLA	AHDCNN
10	24.5	36.7	47.7	56.7	69.8	80.2
20	26.7	38.9	50.1	62.3	74.5	84.5
30	27.9	40.1	48.2	59.8	79.2	87.2
40	34.5	39.8	54.4	64.5	78.6	90.4
50	35.7	43.2	55.9	62.9	77.2	97.3

1)**F1 Score**

Precision: By evaluating the actual beneficial effects of the anticipated ones, this keeps track of the model's correctness. The ratio of accurately predicted positive items to all predicted things is:

$$Precision = \frac{True\ positive}{true\ positive + False\ positive}$$

(24)

Recall: The model counts the number of true positive values that are recorded and classified as positive.

$$/Recall = \frac{True\ positive}{True\ positive + False\ Negative}$$

(25)

The precision and recall function is the F1-score. If a precise- recall balance is necessary, the balance is established.

$$F1 = 2 \times \frac{Precision \times Recall}{Precision + Recall}$$

(26)

The suggested AHDCNN method's f1-score is displayed in Figure 9. Comparing the suggested AHDCNN approach to the current NCA, DNN, HNN, RNN, and EMS-DLA methods, a high precision-recall ratio is obtained.The F1-score for the suggested AHDCNN approach is displayed in Table 2. Dietary Adjustments for Renal Disease and Walser Formulae
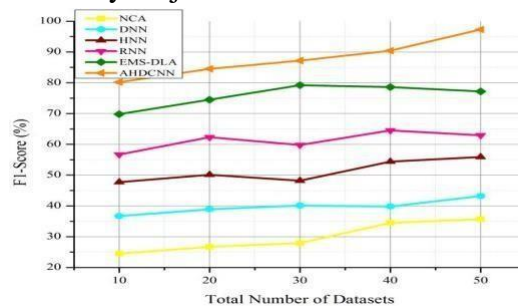

FIGURE 9-F1 Score analysis with numerical results

TABLE 2-F1 Score evaluation

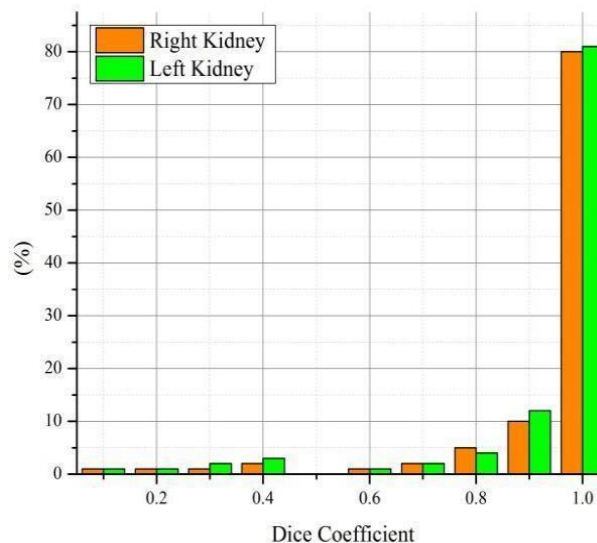| Total Number of datasets	NCA	DNN	HNN	RNN	EMS-DLA	AHDCNN
10	24.5	36.7	47.7	56.7	69.8	80.2
20	26.7	38.9	50.1	62.3	74.5	84.5
30	27.9	40.1	48.2	59.8	79.2	87.2
40	34.5	39.8	54.4	64.5	78.6	90.4
50	35.7	43.2	55.9	62.9	77.2	97.3

FIGURE 10: Dice COEFFICIENT ratio.

demonstrated the greatest outcomes with the highest precision and the fewest biases. Compared to other current approaches, the suggested AHDCNN method has a high precision and recall ratio.

DICE COEFFICIENT RATIO:

The Dice Index has contrasted the automatic segmentation results, including the detection step, with the ground truth. Figure 10 displays the histograms of the two kidney rats. The appropriate identification and Eighty percent of the kidneys have undergone segmentation (Dice > 0.90). The algorithm failed only 6% of the time (Dice < 0.65). The implementation takes about 10 seconds in total. This statistical analysis examines how similar two samples are to one another:

FIGURE 11: Receiver operating curve with AUC values.

Eighty percent of the kidneys have undergone segmentation (Dice > 0.90). The algorithm failed only 6% of the time (Dice < 0.65). The implementation takes about 10 seconds in total. This statistical analysis examines how similar two samples are to one another:
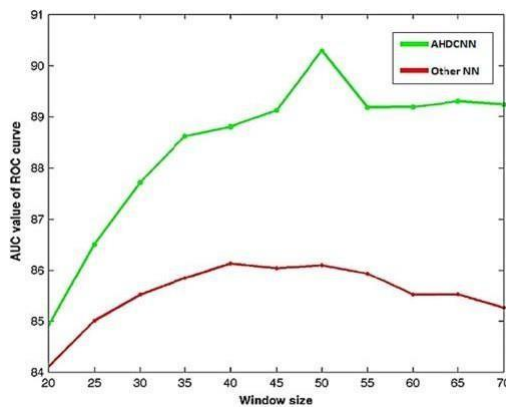
RECEIVER OPERATING CURVE ROC:

The effectiveness of the suggested model at every classification threshold is shown by the ROC curve (ROC-curve). This is an illustration of the ratio of true positives to false positives (TPR vs. FPR). AUC is the area under the (0, 0) to (1, 1) integrated ROC curve. It provides the overall measurement of all potential classification thresholds. AUC ranges from 0 to 1. A 100% right version will have an AUC value of 1.0, whereas a 100% erroneous classification will have an AUC value of 0.0. It is appealing for two reasons: first, it assesses the model's predictability rather than absolute values thanks to its invariant scale. Second, it has an invariable classification threshold as it checks the accuracy of the model regardless of the threshold. The ROC curve's AUC values for the suggested AHDCNN approach are displayed in Figure 11. The following equations represent the TPR and FPR ratio.

$$TPR = \frac{True\ positive}{True\ positive + False\ Negative} \quad (28)$$

$$FPR = \frac{False\ positive}{False\ positive + True\ Negative} \quad (29)$$

LOSS OF FUNCTION ON AHDCNN:

When evaluating the effectiveness of AHDCNN in the kidney disease dataset, the loss function is helpful. Based on an evaluation using the sensitivity and specificity scale, the low loss function value suggests that the AHDCNN technique
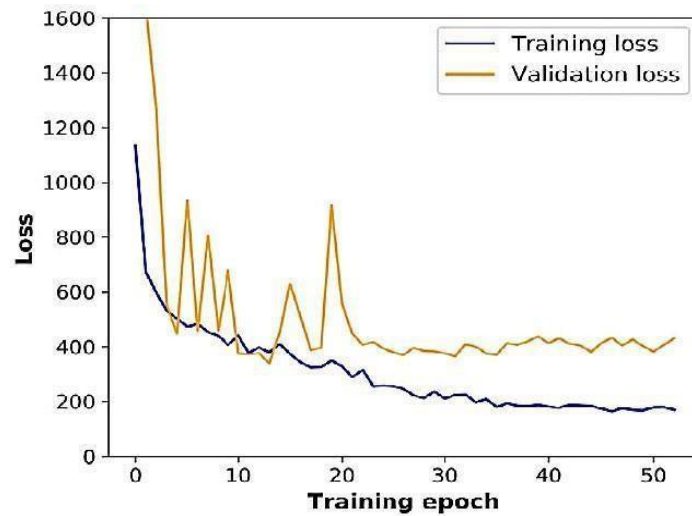
FIGURE 12: Loss function of AHDCNN:

more accurately distinguishes between normal and pathological renal disease. The sensitivity of the AHDCNN procedure is one way to assess its accuracy. The following is the estimate:

The suggested AHDCNN method's loss function and cross-entropy values are displayed in Figure 12.As a result, the loss function has been examined using the following criteria: low contrast between the renal and other abdominal images, especially higher gradient strengths and lengths; kidney movement due to breathing and heartbeats; and changes in kidney form due to anatomical variations among patients.

The degradation issues that emerge as deep networks converge—that is, the growing complexity of precision loss and degradation—are addressed by deep residual learning. Rather than fitting into a predefined context frame, the residual network makes the layers stack directly to fit into the map. The experimental findings accomplish precision with a significant increase in depth and enhance residual network optimization (Figure 13).

CONCLUSION

In this research, the Adaptive Hybridized Deep Convolutional Neural Network (AHDCNN) for Chronic Kidney Disease (CKD) early diagnosis and prediction is presented. The unique subtypes of lesions in kidney cancer are recognized from CT scans using a deep learning algorithm. The median value estimate will be used to replace the missing value after the obtained data has been first examined. The noise-free data is used to identify several kidney disease-related variables, which are then fed into a classifier designed to detect changes in kidney patterns. The system trains features in each hidden layer by calculating the weight and bias value. The deep-belief network's numerous layers further teach the trained features to identify irregular patterns. Effective double-training to prevent kidney disease involves making effective use of the learning and activation process. The data distribution and regression analysis are then established. The deeper learning method and ROIs provided by radiologists are the foundation of the suggested strategy, which has demonstrated encouraging outcomes in the classification of renal cell subtypes.

REFERENCES

1. J. Lin, ''A comparison of prediction equations for estimating glomerular filtration rate in adults without kidney disease,'' J. Amer. Soc. Nephrology, vol. 14, no. 10, pp. 2573–2580, Oct. 2003.
2. S. Anderson, J. B. Halter, W. R. Hazzard, J. Himmelfarb, F. M. Horne,
3. G. A. Kaysen, and J. R. Ashworth, ''Prediction, progression, and outcomes of chronic kidney disease

in older adults,'' J. Amer. Soc. Nephrol., vol. 20, no. 6, pp. 1199–1209, 2009.

4. H. Bang, S. Vupputuri, D. A. Shoham, P. J. Klemmer, R. J. Falk,

5. M. Mazumdar, and A. V. Kshirsagar, ''SCreening for Occult REnal Disease (SCORED): A simple prediction model for chronic kidney disease,'' Arch. Internal Med., vol. 167, no. 4, pp. 374–381, 2007.

6. N. Tangri, G. D. Kitsios, L. A. Inker, J. Griffith, D.

7. M. Naimark, S. Walker, and A. S. Levey, ''Risk prediction models for patients with chronic kidney disease: A systematic review,'' Ann. Internal Med., vol. 158, no. 8, pp. 596–603, 2013.

8. M. A. Fisher and G. W. Taylor, ''A prediction model for chronic kidney disease includes periodontal disease,'' J. Periodontol., vol. 80, no. 1, pp. 16–23, Jan. 2009.

9. D. E. Weiner, H. Tighiouart, E. F. Elsayed, J. L. Griffith, D.

10. N. Salem, A. S. Levey, and M. J. Sarnak, ''The framingham predictive instrument in chronic kidney disease,'' J. Amer. College Cardiol., vol. 50, no. 3, pp. 217–224, Jul. 2007.

11. C. D. Owens, K. J. Ho, S. Kim, A. Schanzer, J. Lin, E. Matros, M. Belkin, and M. S. Conte, ''Refinement of survival prediction in patients undergoing lower extremity bypass surgery: Stratification by chronic kidney disease classification,'' J. Vascular Surg., vol. 45, no. 5, pp. 944–952, May 2007.

12. L. Jena and N. K. Kamila, ''Distributed data mining classification algo- rithms for prediction of chronic-kidney- disease,'' Int. J. Eng. Res. Technol., vol. 4, no. 11, pp. 110– 118, Nov. 2015.

13. G. S. Collins, O. Omar, M. Shanyinde, and L. M. Yu, ''A systematic review finds prediction models for chronic kidney disease were poorly reported and often developed using inappropriate methods,'' J. Clin. Epidemiol., vol. 66, no. 3, pp. 268–277, 2013.

14. I. Lazich and G. L. Bakris, ''Prediction and management of hyperkalemia across the spectrum of chronic kidney disease,'' Seminars Nephrol., vol. 34, no. 3, pp. 333–339, May 2014.

15. A. Chang and H. Kramer, ''Should eGFR and albuminuria be added to the Framingham Risk Score chronic kidney disease and cardiovascular disease risk prediction,'' Nephron Clin. Pract., vol. 119, no. 2, pp. c171–c178, 2011.

16. K. D. Liu, W. Yang, A. H. Anderson, H. I. Feldman, T. Hamano, and M. S. Simonson, ''Urine neutrophil gelatinase–associated Lipocalin levels do not improve risk prediction of progressive chronic kidney disease,'' Kidney Int., vol. 83, no. 5, pp. 909–914, 2013

17. I. E. E. Kocyigit, A. Unal, M. H. Sipahioglu, B. Tokgoz, C. Utas, ''Role of neutrophil/lymphocyte ratio in prediction of disease progression in patients with stage-4 chronic kidney disease,'' J. Nephrol., vol. 26, no. 2, pp. 358–365, 2013.

18. V. B. Kolachalama, P. Singh, C. Q. Lin, D. Mun, J. M. Henderson, J. M. Francis, D. J. Salant, and V. C. Chitalia, ''Asso- ciation of pathological fibrosis with renal survival using deep neural net- works,'' Kidney Int. Rep., vol. 3, no. 2, pp. 464–475, Mar. 2018.